Rock Mech Rock Eng (2009) 42:631–665
DOI 10.1007/s00603-008-0010-4

ORIGINAL PAPER

Advanced Geostructural Survey Methods Applied to Rock Mass Characterization

A. M. Ferrero · G. Forlani · R. Roncella · H. I. Voyat

Received: 20 December 2006 / Accepted: 7 April 2008 / Published online: 21 June 2008

Abstract The location and orientation of rock discontinuities, which are traditionally obtained from geological surveys with obvious drawbacks (safety, rock face accessibility, etc.), may also be derived from a detailed and accurate photogrammetric or laser scanning survey. Selecting from the point cloud determined on the rock face a set of points distributed on a particular discontinuity, location, dip, and dip direction can be computed from the least-squares estimate of the plane interpolating the set of points. Likewise, the normal vector to the surface may be computed from an interpolation or approximation of the surface by appropriate functions. To become a real alternative (both in terms of productivity as well as accuracy) to a traditional survey, interactive or automated software tools are necessary, to allow the efficient selection of the point sets on the discontinuities or the interpretation of the normal vector pattern. After introducing the two best technologies available today for data acquisition and their performance, the paper presents an approach, based on the random sample consensus (RANSAC) procedure, to the segmentation of the point cloud into subsets, each made of points measured on a discontinuity plane of the rock face. For each subset, the plane's equations coefficients are first determined by robust estimation and then refined by least-squares estimation after outlier removal. The segmentation algorithm has been implemented in RockScan, a software tool developed to facilitate the interaction with the point cloud in the identification of the discontinuities; rather than using the three-dimensional (3D) data, selection of regions of interest is performed on oriented images of the rock face. Finally, application of RockScan to four different test sites is discussed and results presented. The sites differ in size (from tens to

A. M. Ferrero (✉) · G. Forlani · R. Roncella
University of Parma, Parma, Italy
e-mail: annamaria.ferrero@unipr.it

H. I. Voyat
Fondazione Montagna Sicura, Courmayeur (Aosta), Italy

hundreds of meters), rock surface characteristics, and the technology used to produce the point cloud (in three cases photogrammetry, in the fourth laser scanning), giving the opportunity to test the methodology in different contexts. In the first and in the fourth site an extensive traditional survey has been performed, providing reference data to validate the RockScan results.

Keywords Rock mass characterization · Geostructural survey · Advanced techniques

1 Introduction

A geostructural survey devoted to a systematic and quantitative description of rock discontinuities is a fundamental part of the study of the stability conditions of a rock mass. Discontinuity sampling can be applied to rock faces, natural or artificial such as excavations, or on boreholes depending on the available data. Discontinuity properties to be measured include dip, dip direction, length, spacing, roughness, persistence, aperture, filling, and termination (Priest 1993).

Traditionally, surveys are performed with a geological compass, measuring dip and dip direction directly on the discontinuity. In several cases, this can be difficult because:

- discontinuities or even the rock faces themselves cannot be easily accessed, or their size is so large that on-site data acquisition may be time consuming and expensive;
- rock masses are so heavily fractured and unsupported that just being close to the slope can be dangerous.

Surveys are carried out on scanlines or in a more detailed way through observation windows. A correct joint geometry representation is suggested by the ISRM (1978) based on the collection of a sample that must be representative of the entire joint population (Davis 1986; Kulatilake et al. 1993). Relative orientation between discontinuity and scanline can lead to bias error (Terzaghi 1965; Cruden 1977; Priest and Hudson 1976, 1981). Window sampling provides data of better quality compared to scanlines, because it reduces inherent bias errors. However, to reduce bias by an adequate sampling methodology or by applying bias correction algorithms, the collection of a large amount of data is required. As pointed out above, this may not be feasible or cost effective with a compass survey.

In some cases, fracturing aspects cannot be directly observed in the fieldwork by the geologist. Think, for instance, of very large slopes, where traditional sampling would need the help of professional climbers and where important fracture systems may go unnoticed unless suitable aerial images are available, because little can be seen of the face from the bottom.

In order to set up a 3D geometrical model of the rock mass, both the topographic description of the rock slope and its geostructure are needed. An alternative to traditional surveys, capable of overcoming in many cases the problems outlined above, is to derive dip and dip direction, as well as the location of the

discontinuities, from a very detailed topographic survey, i.e., by measuring a very dense point cloud on the rock surface. If a set of points surveyed on a particular discontinuity is selected, dip and dip direction can be computed from the equation of the best fitting plane (i.e., from the unit vector perpendicular to the plane); if a digital surface model of the rock face is used (e.g., a triangulated mesh), the same applies for calculating the average unit normal vector of the inspected region. Therefore, the survey will provide not only the slope topography but will also allow the identification of the discontinuities in terms of position on the slope and orientation, spacing, persistence, and joint hierarchy.

Besides overcoming the limitations outlined above, other advantages are apparent:

- a larger number of measurements can be collected on the slope, including where inaccessible, with much less effort than with direct measurements;
- the evaluation becomes less subjective: since more information on the slope is collected, analysis can be performed on the whole rock surface rather than on a limited number of scanlines decided by the geologist;
- additional measurement can be performed at any time, to refine the evaluation or solve ambiguities of interpretation.

Different technologies may be applied to acquire 3D data: in the past attempts were made using total stations (Feng et al. 2001), but the most appealing techniques nowadays are stereo photogrammetry and laser scanning. With a proper design of the survey, both can deliver accurate (typically 1–5 cm) and closely spaced points, ensuring that the relevant features of the rock face are captured in the point cloud. As far as rock surface roughness is concerned, the same techniques (using higher resolution and then higher accuracy) can provide adequate results. To become a real alternative (both in terms of productivity as well as accuracy) to a traditional survey, interactive or automated software tools are necessary, to allow the efficient selection from the point cloud of the points laying on the discontinuities. A point cloud can be handled by any 3D modeling software; a continuous surface may be generated using simple triangular irregular networks (TINs) or more sophisticated parametric representation such as nonuniform rational B-splines (NURBS). However, selecting the points on a discontinuity directly from the point cloud or even from a surface visualization in 3D is not easy; pictorial information is necessary and can be added directly to the points of the cloud or overlaid onto the surface using oriented images (i.e., images whose position and attitude with respect to the point cloud is known). Another option is to manage the interaction with the point cloud indirectly, using oriented images; in this case, if a discontinuity is contoured on an image of the rock face, the points are selected by back-projection of the point cloud onto the image.

No matter how the selection of points is implemented, automation of the process would increase productivity: ideally, a segmentation of the whole point cloud into disjoint sets of points, each corresponding to a discontinuity, would make the process very fast, exploiting all of the information hidden in the point cloud. Irrespective of the technology used in data acquisition, to the best of the authors' knowledge, currently no established fully automated method exists. While in several cases results may be correct, a degree of interaction and/or integration by manual measurements is normally necessary.

This paper presents an approach, based on the RANSAC algorithm (Fischler and Bolles 1981), to the semi-automatic segmentation of a point cloud to extract the discontinuities of a rock face; the algorithm is implemented in an interactive software program that takes as input a point cloud as well as oriented images. By contouring on the image an area with one or several discontinuities, their position, dip, and dip direction are automatically computed.

Once both the topography of the slope and the geostructure are known, a kinematic analysis can be performed. Among other factors, the blocky nature of the rock mass strongly influences the stability conditions of the slope; consequently, methods that take the discontinuities into account are often applied.

A discussion of methods to perform stability analysis in a discontinuous medium is outside the scope of this work (see Barla and Barla 2000, 2001; Jing and Hudson 2002; Jing 2003; Ferrero et al. 2004). Two of the most commonly used methods in rock mechanics, the limit equilibrium method (LEM) and the discrete element method (DEM), are mentioned to show how different procedures can be applied to determine rock slope stability.

With both approaches rock block geometry must be determined. When the discontinuities are known both in terms of orientation and location we can reconstruct the rock mass in a deterministic way while, when we have just the orientation of the planes, a statistic reconstruction of the rock mass can be performed. When discontinuities are not directly observable on a rock outcrop borehole sampling is necessary. In this case statistical reconstruction of the rock mass must be carried out. Geometrical reconstruction of rock masses is then a combination of data coming from different sources properly treated by statistical analysis of and mathematical assumptions about the distribution of discontinuity trace length and size, and discontinuity shape (Zhang and Einstein 1998, 2000). Examples of the geometrical rock mass reconstruction phase, based on detailed surveys, are also reported herein.

The outline of the paper is as follows: in Sect. 2 alternative methods to the compass-based survey are reviewed; Sect. 3 discusses accuracy issues connected to noncontact survey methods such as photogrammetry or laser scanning; Sect. 4 illustrates methods for the segmentation of the point cloud, highlighting the challenges for a full automation of the procedure; then, the software program RockScan, developed by the authors for the semi-automated identification and extraction of discontinuities, is presented. After the description of the segmentation strategy implemented, the procedure for manual or semi-automatic extraction of discontinuities through the selection of linear scanline or sampling windows is illustrated. Finally, Sect. 5 discusses the results obtained with RockScan in several test cases, using data acquired by photogrammetry or by laser scanning.

2 Geostructural Survey by Noncontact Measurements

Images recorded on site are not just made for documentation and archiving; rather they are a primary source of information. Photo analysis or photogrammetric methods, complementary or alternative to the compass survey, have been developed

in the last three decades. Broadly speaking, they can be divided into monoscopic or stereoscopic methods. In the former group, measurements are made directly on the image space and transferred, under some hypothesis on the relationship between camera and rock face orientation, to the object space (the rock surface). In the latter group of methods, the information on rock fracturing aspects is extracted directly from the interpretation of the 3D data obtained by stereo photogrammetry (i.e., a point cloud, rather than the image); in this respect, laser scanning is the most recent technique to join the latter group. Images still play a role, but only to make interaction with the 3D data easier. In both monoscopic and stereoscopic approaches, partial or full automation of feature identification and measurements is pursued: in the former, using image analysis; in the latter, using computational geometry, cluster analysis, and robust statistics.

The relationship between discontinuity sets in terms of joint hierarchy and different kinds of joint terminations, which can strongly influence the rock mass mechanical behavior, can be observed on images as discontinuity traces. Tsoutrelis et al. (1990) and Crosta (1997) built manually discontinuity trace maps from single images; however, manual measurements are time consuming. A real step ahead in the geostructural survey was performed with the development of a method for automatic recognition of discontinuities on images. Reid and Harrison (2000) identify traces as ravines in the image brightness surface, classifying pixels based on gradient and curvature analysis and using a line-following algorithm from manually selected seed points. Hadjigeorgiou et al. (2003) review previous work on automatic trace detection and compare the performance of several edge and line detection algorithms. Overall, the poor reliability of the methods was highlighted, as well as the strong dependence of the results on rock texture, illumination conditions, and threshold settings, resulting in meaningless segments or excessive fragmentation.

To solve the ambiguities in labeling segments, Lemy and Hadjigeorgiou (2003) and Grenon et al. (2004) measured several geometric and radiometric parameters of the image segments, assuming discrimination in parameter space to be achievable (i.e., that meaningless image segments can be discarded and those corresponding to real traces retained). To this aim, they use neural networks, reporting a good success rate; however, it is not clear whether training needs to be repeated for every project (or even in any image). In order to improve the detection rate they controlled lighting in an underground environment and set threshold values for edge and line detection low; while illumination normal to the face is the best suited to locate lines, it is suggested to take several images from different oblique illumination directions for edges (Hadjigeorgiou and Lemy 2005). Successful identification of discontinuities traces, including their length, spacing, and positions, has been shown in two case studies in underground mining; an example in an open environment, although very simple, required adjustment of the processing parameters in order not to miss an important family. The need to control illumination makes the method of limited use in daylight; besides, the claim that the method does not require contact with the rock is somehow contradicted by the need to come close to it to provide oblique illumination; more crucially, to determine discontinuity orientation, they have to measure directly, for each main family, at least four dips and dip directions.

Kemeny and Post (2003) derive 3D fracture orientations (dip and strike) from 2D fracture trace information gathered from digital images of exposed rock faces. It is assumed that the orientations of the rock face and the camera are known, that the rock face is relatively flat, and that the camera is positioned perpendicular to the strike of the rock face (but not to the dip). The method estimates the constant K and the mean value of a Fisher probability density function for joint orientation data; from synthetic data it has been shown that, if the trace appears in two nonparallel rock faces, the accuracy of dip and dip direction is very good (about 1°). Traces are delineated manually or semi-automatically by extracting lines with the well-known Hough transform.

Apart from trace discontinuity maps, truly 3D information can be extracted from monoscopic vision only if certain geometric conditions on the relative orientation between the camera and rock face and on rock face shape, not always met in practice, are satisfied. Stereoscopic methods combine information from two pictures of the same rock face, allowing direct extraction of 3D information (Hagan 1980; Harrison 1993).

Gaich et al. (2004, 2006) use stereo photogrammetry using both a digital panoramic camera (to maintain high resolution on the whole object) and a less expensive digital camera (for small areas). After the digital terrain model (DTM) of the rock surface was generated using triangulation, images were overlaid on the DTM and a graphical interface allowed the user to measure the position, dip, and dip direction of discontinuities as well as distances and areas. The surface normal in a given position was computed from the mean orientation values of the neighboring surface elements. Discontinuity orientation from traces could be measured if the corresponding 3D polyline effectively defined a plane. Normal stereo imaging geometry is used, which does not yield homogeneous accuracy and might have unfavorable angles with respect to the surface normal unless simple rock shapes are imaged. Measurements were interactive only, which is not very efficient when complex rock structures have to be sampled. Birch (2006) discussed the application of photogrammetry to rock face characterization, stressing the need for appropriate image block design and accuracy issues. Automatic image orientation and generation of DTM mass points by digital image correlation was reported, but automation of discontinuity extraction was not mentioned.

In recent years, laser scanning (Kemeny et al. 2003, 2006; Dolan 2006) has emerged as an alternative to photogrammetry to acquire dense point clouds on rock faces.

An important point should be stressed here: using both photogrammetry and/or laser scanning the accuracy in discontinuity plane interpolation depends on an appropriate sampling of the discontinuity itself: the data must ensure that the plane orientation is captured accurately (see Sect. 3.1). When only discontinuity traces mark a family (e.g., in sedimentary rocks, or if failure, erosion, denudation, excavation, etc., has occurred) then a different technique should be used (see Kemeny and Post 2003 for instance).

3 Three-Dimensional Data Acquisition

To be competitive with the compass survey, alternative methods for determining points on the discontinuities must satisfy a number of conditions:

- points should be measurable on every main or significant discontinuity in the rock face;
- the accuracy of dip and dip direction computed from plane fitting should at least match that of the compass;
- automation of point measurement, identification of discontinuity planes, and computation of the geostructural parameters should be a priority, in order to limit the total survey time (field and office work) and increase efficiency;
- the method should not require direct access to the rock face;
- costs should be lower overall than those of a comparable traditional survey.

3.1 Accuracy of Dip and Dip Direction Determined by Noncontact Methods

As pointed out in the previous section, advantages of noncontact over the traditional method should include better measurement accuracy. In this section, a mathematical and stochastic model is presented that describes the accuracy of dip and dip direction determination as a function of the most relevant parameters: the accuracy of 3D coordinates of the points surveyed on the discontinuity plane, the orientation (dip and dip direction) of the plane, the size and shape of the plane, and the number of points measured on the discontinuity. Numerical tests have been executed, varying these parameters, in order to understand which are the most important and whether critical cases may arise. Due to the number of parameters involved, some simplifications or assumptions have been made, but the results are believed still to capture the trend.

The discontinuity plane is represented by a rectangular surface on which points have been measured by laser scanning or photogrammetry. To account for the influence of the discontinuity shape, the base b has been kept fixed, while the ratio b/h (where h is the rectangle height) has been varied from 1/5 to 5 to represent elongated shapes in height and width (as well as a square). The measurement points are distributed on the rectangle on a square grid; the grid spacing has been varied as a percentage of the shortest rectangle side, from 10 to 100%. Depending on the spacing, therefore, the number of points on the plane varies from 4 to 121 for a square shape and from 12 to 561 for b/h equal to 1/5 and 5 (Table 1).

The theoretical measurement accuracy of a point is represented by an error ellipsoid. As long as a single discontinuity plane is considered, the error ellipsoids of the points surveyed on it by photogrammetry or laser scanning are very much the same for all points. This is because in both measurement techniques the spatial function describing the error behavior is smooth, so the effects of its variation in a few meters on dip and dip direction accuracy are negligible. The influence of the orientation of the ellipsoid in space has been implicitly taken into account by varying the dip and dip direction of the plane.

In most cases, for photogrammetry as well as laser scanning, the semi-axes of the ellipsoid are different; some tests were made, changing their ratio up to 1:3, but the effect was not found to be very important: therefore, in the following, homogeneous accuracy in 3D has been assumed. Under this assumption, the accuracy of both parameters does not depend on the dip direction of the discontinuity.

Table 1 Number of grid points measured on each rectangle as a function of grid spacing; the point density increases with decreasing values of the factor k and of rectangle height

Rectangle base, $b = 1$; grid spacing = $k \times \min(b, h)$			
Rectangle height, h	0.2	1	5
Grid spacing ($k = 0.1$)	0.02	0.1	0.1
# Pts	561	121	561
Grid spacing ($k = 0.2$)	0.04	0.2	0.2
# Pts	156	36	156
Grid spacing ($k = 0.5$)	0.1	0.5	0.5
# Pts	33	9	33
Grid spacing ($k = 1$)	0.2	1	1
# Pts	12	4	12

3.1.1 Estimation of the Accuracy of the Components of the Unit Vector Normal to the Discontinuity Plane

The accuracy of dip and dip direction as a function of measurement accuracy has been computed by variance propagation within a generalized least-squares model:

$$Dy = Ax + d$$

with parameters x and observables y (Felus 2006). Without loss of generality, the equation of a plane through the origin:

$$ax + by + cz = 0$$

has been considered; the functional model is of the form $F(y, x) = 0$ and must be linearized with respect to the observables as well as with respect to the parameters. We therefore have

$$D = \frac{\partial F}{\partial y}; \quad A = -\frac{\partial F}{\partial x}; \quad d = -F(x_0, y_0),$$

where D contains the parameters of the plane and A the coordinates of the points which define the plane, while x_0 and y_0 are, respectively, approximations to the parameters and point coordinates. The stochastic model is defined by the covariance matrix of the observations C_{YY}, which is taken as block diagonal, neglecting correlations between measurement points (as well as, as discussed above, those between the coordinates of a point).

Since the design matrix A is rank deficient due to the homogeneous form of the plane's equation, an additional constraint must be added; because of their geometrical meaning (the components of the unit vector normal to the plane) the nonlinear constraint $a^2 + b^2 + c^2 = 1$ should apply. This is enforced by adding a pseudo-observation equation of the constraint, expressed in linearized form, to the equation system and assigning it a very large weight.

The theoretical accuracy of the parameters is given by the covariance matrix C_{xx} computed by covariance propagation:

$$C_{xx} = (A^t(DC_{YY}D^t)^{-1}A)^{-1}.$$

Taking the plane unit normal vector pointing upwards, the dip and dip direction can be expressed as a function of the plane's coefficients as

$$\text{dip} = \arccos(c) \quad \text{dip direction} = k \pm \arctan(a, b),$$

where k is 0° or 180° depending on the quadrant; their accuracy can be derived by a new error propagation, with the full covariance matrix C_{xx}. Note that, as k is a constant, it is eliminated in error propagation.

3.1.2 Discussion

As is apparent, the accuracy of dip depends only on the accuracy of the z component of the vector normal to the plane, while the accuracy of dip direction depends on the accuracy of both the x and y components. Note that the x and y components accuracies are strongly influenced by the z component itself (i.e., subhorizontal planes show poorer accuracies).

Consequently we observe that the accuracy in estimating the plane dip direction is strongly influenced by the plane dip angle for nearly horizontal planes (below 30°) as well.

The accuracy of dip and dip direction will mainly depend on two factors: the ratio between the point accuracy and their average distance, and the roughness of the actual rock surface. It should be obvious that large smooth plane surfaces can be determined very well, even with points of relatively poor accuracy, provided that they are well apart from each other; if planes are very small or elongated, points must be closely spaced to ensure that at least some fall in each plane; in such cases, however, even small uncertainties may lead to errors of several degrees in dip and dip direction. To obtain meaningful guidelines for survey design several simulation with the above statistical approach have been performed, using different face shapes and varying the resolution (i.e., the density of points on the face itself).

Figure 1 shows results for the case of a plane with a ratio length width (b/h) of 5, 1, and 0.2, a precision of 5% ($\sigma_{xx}/b = 0.05$), and a dip direction of 90°. On the right, dip direction accuracy variation with plane dip is exhibited, whilst on the left dip accuracy variation with the plane dip is shown.

The lower precision determining the dip direction for nearly horizontal planes becomes more evident when the number of acquired points is smaller. Dip accuracy appears to be less influenced by dip plane variation. In all the examined cases accuracy improved by acquiring a larger number of points.

The graphs in Fig. 1, as already stated, can be used as a guide in survey design to obtain a certain accuracy in the dip and dip direction estimation: for a discontinuity of a given dimension and for a fix precision we can determine the minimum numbers of points to be acquired to obtain the plane dip direction with a certain accuracy. Alternatively, the minimum dimension of an outcropping discontinuity

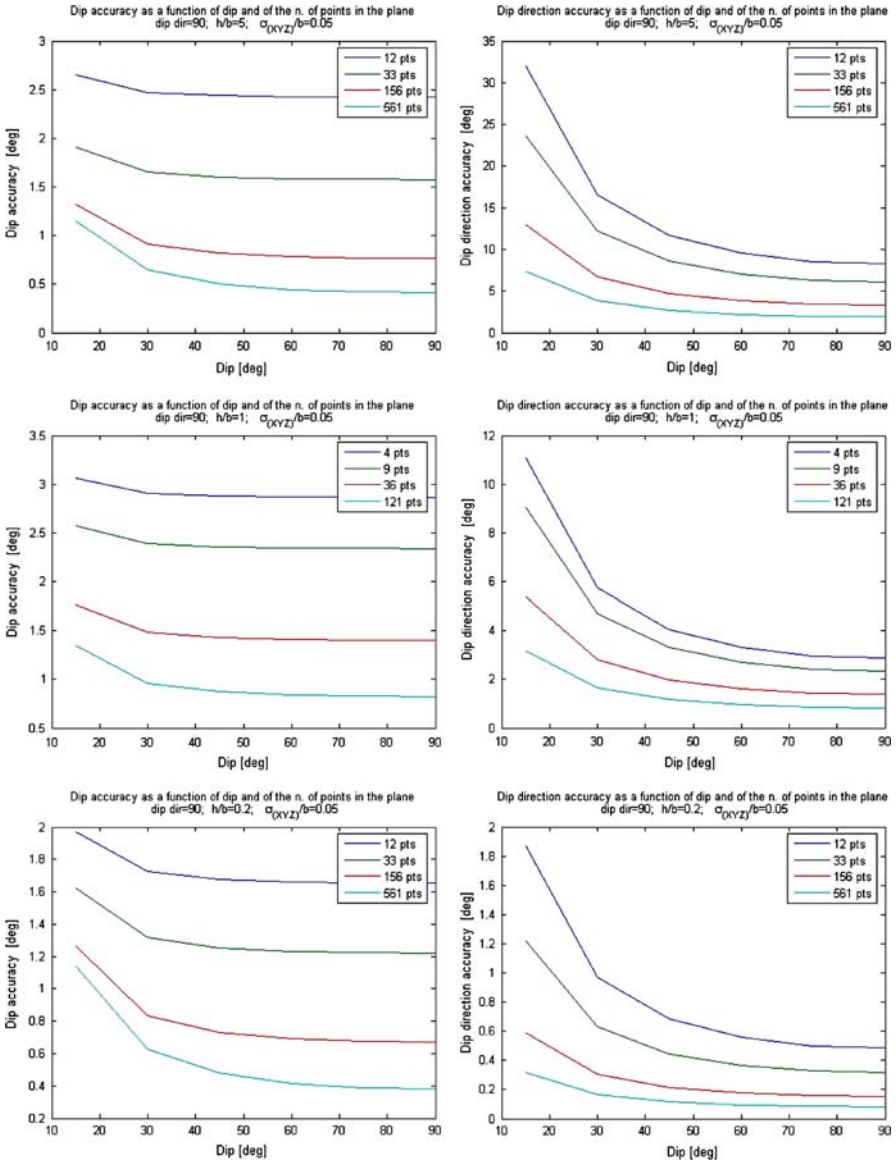

Fig. 1 Dip and dip direction accuracy computation for different plane shape (*b*/*h*) and inclination

necessary to determine its dip and dip direction with a given accuracy can also be defined.

For instance, if a precision equal to 5 cm on a discontinuity of 1 m length is required and the plane has a dip of 20° a minimum number of 156 points is needed for a plane with *b*/*h* of 5, whereas only 4 points are required for a square plane (Fig. 1).

As is apparent from the literature survey in the previous section, today photogrammetry and terrestrial laser scanning are the two competing techniques with the potential to address all the above listed requirements.

3.2 Photogrammetry

Photogrammetry provides the 3D coordinates of points with predictable accuracy from stereo or multiple images (i.e., from images of the same scene taken from different viewpoints). The accuracy of the coordinates depends on a number of factors, which must be accounted for when designing the three stages of any photogrammetric survey: camera calibration, image orientation, and object restitution. Camera calibration, to be repeated periodically, determines lens and interior orientational camera parameters in the laboratory. The exterior orientation parameters (camera position and attitude with respect to the object reference system at every station) are computed indirectly by measuring the image coordinates of points with known object coordinates (GCP, ground control points), surveyed, e.g., by total stations. For a single stereo pair, four GCPs are necessary to ensure good accuracy; with large rock faces, for which several images are necessary, simultaneous orientation of a whole block of overlapping images allows for a very significant reduction of the number of GCPs, with negligible loss of accuracy, by measuring tie points on the images (Kraus 1993). Using feature-based image matching and structure from motion (Roncella et al. 2005; Birch 2006) tie points can be extracted and matched automatically, therefore image orientation can be obtained without any manual measurement. Orientation parameters can also be determined directly, by fixing a global positioning system (GPS) receiver, integrated with an inertial measurement unit (IMU), to the camera (Vallet et al. 2000); in this case, no GCPs are necessary. However, a GPS signal must be available almost continuously for the orientation data to be accurate: such systems are, therefore, best used either airborne or where satellite visibility from camera stations is not severely limited by obstacles such as high vegetation or by the rock faces themselves.

With a well-calibrated camera and accurate image orientation, the accuracy of point determination improves:

- the closer the angles between homologous rays are to 90° (in a stereo pair, this depends on the ratio of the distance between the two camera stations with respect to the camera–object distance);
- the larger the image scale (the ratio between the camera focal length and the camera–object distance);
- the higher the accuracy of the measurement on the image (with digital images of natural surfaces, normally in the range 0.2–1 pixel).

The restitution may be executed manually by an operator or automatically. The former option exploits the ability of the operator to select the minimum number of points necessary for a reliable identification of a discontinuity plane; the latter exploits the capabilities of image matching algorithms, such as least-squares matching (Grün 1985), to compute several thousand points in seconds, but has to

deal later with outlier removal and the identification of planes within the point cloud; robustness, as well as accuracy in object space, can be improved by using multi-image matching (Grün and Baltsavias 1988).

3.3 Laser Scanning

Light detection and ranging (LIDAR) data are a primary data source for DTM generation; they can be operated either from ground, as a standalone system, or in airborne systems, in the latter case integrated with a navigation system. The main components of a LIDAR system are a laser telemeter and a scanning mechanism. Two distance measurement principles are used: most short range (up to 50–100 m) lasers operate with the phase-shift (continuous-wave) principle; long-range systems (which are less accurate) normally operate with the pulse (time-of-flight) principle. Terrestrial and aerial laser scanners differ in the way the distance information is combined to provide the target position.

In most terrestrial scanners, scanning is obtained by combining a rotating mirror and a rotating head mounted on orthogonal axes; the polar coordinates of the target are then converted to am instrumental frame with its origin at the instrument centre, z-axis along the rotation axis, and x-axis in an arbitrary direction. There are a number of systems available, suited to different applications. In the context of point cloud generation for rock faces, the maximum operating ranges of current scanners vary from about 100 m up to 800 m and above, with accuracies of 3D coordinates in the range 0.5–3 cm and scanning speed from 2,000 to 12,000 pts/s (http://www.leica-geosystems.com, http://www.optech.com, http://www.riegl.com, http://www.trimble.com, accessed 6 March, 2006). Accuracy in range decreases with target distance and target reflectivity; because of beam divergence (on the order of 0.2–0.25 mrad) and of the optics aperture, the laser footprint is a disc of varying diameter (up to a few centimeters), and therefore the measured range is in fact an average value; a large incidence angle to the surface normal leads to ellipticity of the disc and increasing uncertainty of the measurement.

Angular scanning resolutions are on the order of 100 μrad and allow for a very high sampling density on the object in relatively short acquisition times, resulting in millions of points measured on the object surface; it should be noted, however, that actual angular resolution depends also on the beam divergence (Lichti and Jamtsho 2006).

Since the measured coordinates refer to an instrumental reference system, targets are set on reference points to compute a spatial (conformal) transformation from the instrument to the object frame. Likewise, if several scans have to be joined to complete the DTM of a large area or to provide different viewpoints to avoid occlusions, a transformation to a common reference is necessary. To this aim, point-based registration (accurate and reliable) or surface matching (automated but less accurate) can be applied. In the former method, various analytical approaches (conformal, procrustean, etc.) are available that allow simple pairwise registration of scans or simultaneous registration (a technique similar to block adjustment in photogrammetry) of all scans. The best results are obtained by using as common points in the transformation highly reflective (and often spherically shaped) targets,

well distributed on the scan area, which can be detected automatically and very precisely in the point cloud. In the latter methods, such as iterative closest point (ICP, see Besl and McKay 1992), no common targets are needed, since the algorithms use the (triangulated) surface of overlapping scans to find the transformation parameters best fitting the two surfaces in the overlapping area. Seed point may be necessary to provide a preregistration, though.

Airborne laser scanners determine the ground position of points with an accuracy of 10–20 cm in elevation and 15–50 cm horizontally, depending on the flight height and surface characteristics. The main components of an airborne LIDAR system are a scanning laser telemeter and a GPS/IMU system. The sensor position and attitude is interpolated at the time each pulse is emitted, so that the 3D coordinates of each echo received back from a single pulse are computed. The system may operate from helicopters or airplanes. The combination of the forward movement of the aircraft and the the cross-flight movement by an oscillating mirror results in a swath of terrain being sampled. The point density can be adjusted to be on the order of 10 pts/m^2 or more for high-accuracy DTMs, although it is normally 0.3–1 pts/m^2 in general-purpose DTM production. In this context, although airborne laser scanning hardware characteristics are improving, this technique still does not represent a suitable alternative to photogrammetry or terrestrial laser scanning: its dependence on the GPS/IMU accuracy prevents the system from reaching overall accuracies better than 10–20 cm. Should this accuracy level be acceptable (e.g., in the survey of very large structures), there may be some room also for such technique; it must be noted, however, that flying in narrow valleys or close to the bottom of a valley may result in a rather poor GPS constellation and therefore in unreliable results.

4 Automation of Discontinuity Extraction

4.1 State of the Art

As pointed out in the previous section, automation of the extraction of discontinuity planes would sharply increase the productivity of noncontact methods. At least three increasing levels of automation can be conceived. At a very basic level the operator interacts with a 2D or 3D visual representation of the rock face through a graphical user interface (GUI); by pointing to a specific location, the dip and dip direction are computed and stored for later analysis. This is just a replica of what you would do with the compass in the field, with a little automation. At an intermediate level, the extraction process still starts from a GUI, with which the operator singles out parts of the rock face with one or several discontinuities (e.g., enclosing them with a 2D or 3D polyline); after that, the system will take care of discontinuity extraction and parameter computation within the selected areas. At the highest level, once some processing parameters have been set up, an automatic procedure identifies discontinuity planes, computes their parameters, and represents their distribution in a polar plot.

The basic and intermediate levels still rely on the operator's skill and judgment, so are somehow still subjective; full automation derives its objectivity from the

inner logic of the procedure. While examples of the basic level can be found in several commercial programs, full automation is actively being pursued (Roncella et al. 2005; Slob et al. 2005); early results are encouraging, but much progress is still needed in this field.

A degree of interaction today seems the best compromise to exploit the advantages of noncontact methods while still achieving significant time savings compared to on-site surveys. Computation of the dip and dip direction can be performed by working directly on the point cloud or rather on a continuous surface approximation (DTM) of the rock. In the former approach, automatic segmentation singles out the discontinuity planes, dividing the point cloud into subsets, each made of points belonging to a single discontinuity. In the latter, an interpolation (e.g., by triangulation) or an approximation (e.g., by radial basis functions, RBFs) of the rock surface is computed (Slob et al. 2005 for a discussion on interpolation versus approximation and the advantages of RBFs) and the normal to the surface can be computed analytically (for each triangle or at any point on the surface). In practice, due to the high data point density, in interactive measurements the normal is averaged over a set of triangles around the point to reduce the effect of measurement noise; in automatic classification, clustering is used to single out the trends in the data and statistical analysis can be performed to discriminate between dip and dip directions measured on real discontinuities and those surfaces that are not actually formed by the internal discontinuity structure (such as those affected by weathering, fractures through intact rock, soil, etc.).

Robust plane fitting to the point cloud inherently smoothes the measurement noise and is not sensitive to data holes. Triangulation of truly 3D data may lead to wrong connections between points, especially with occluded views and data holes, and is noise sensitive; approximation techniques can manage noise and data holes, but are time consuming and require tuning of the smoothing parameters.

4.2 Segmentation of Point Clouds with RANSAC

In the following an automatic segmentation algorithm to single out the discontinuity planes using robust plane fitting is presented. Since the algorithm works directly on the point cloud, no data structuring (triangulation or approximation) is required.

The equation of a plane in 3D can be expressed as:

$$aX + bY + cZ + d = Ax^{\mathrm{T}} = 0, \tag{1}$$

where $\mathbf{x} = (X, Y, Z, 1)$ are the homogeneous coordinates of a point on the plane determined by the four coefficients $A = (a, b, c, d)$. Given $n > 3$ pts measured on a plane, the determination of the plane's coefficients may be stated as the residual minimization of

$$\left\|XA^{\mathrm{T}}\right\| = \min, \quad \text{subject to } \|A\| = 1, \tag{2}$$

where $\mathbf{X} = [\mathbf{x}_1{}^{\mathrm{T}}, \ldots, \mathbf{x}_n^{\mathrm{T}}]^{\mathrm{T}}$. A least-squares solution can be computed using singular value decomposition (Golub and Van Loan 1989); dip and dip direction can be easily determined (Feng et al. 2001) from the plane's parameters. However, the

least-squares solution of Eq. (2) is statistically optimal (in terms of maximum-likelihood estimation) only if the observations are outlier free; this is never the case with the identification of plane surfaces in point clouds. Indeed, the point cloud can be thought of as being made of points measured on several discontinuity planes and elsewhere (e.g., on vegetation as well as on parts of the rock surface that do not belong to any discontinuity). Therefore, it must first be broken into subsets, each composed of points measured on a discontinuity, before any least-squares technique can be successfully applied.

To this aim, a robust approach based on RANSAC (Fischler and Bolles 1981; Torr and Murray 1997), a widely applied algorithm capable to cope with outlier percentages close to 100%, has been developed (Roncella and Forlani 2005).

Let us assume for a moment that we have a set of points measured with homogeneous accuracy on a single discontinuity plane as well as several outliers. RANSAC looks for the largest subset of data coherent with a given model. To this aim, it randomly selects a model (in our case, a plane) using the minimum number of data necessary to identify it (in our case, three randomly selected points) and finds the size of the set of data coherent with this model. The random selection is repeated several times; the model with the largest score is considered the most likely to represent the correct model (i.e., the plane interpolating the points measured with homogeneous accuracy).

The algorithm starts by randomly sampling three points from the point cloud, so that a specific plane is selected. The distance of each point of the dataset from the plane is computed: if it is less than a threshold, the point belongs to the plane and contributes to the score (cardinality) of the consensus set, otherwise it is considered as an outlier.

The process is repeated N times to ensure (with a probability p) that at least one of the minimal sets is outlier free (i.e., is made of three points all measured on the discontinuity plane). Let ε be the percentage of outliers, then N is given by:

$$N = \frac{\log(1-p)}{\log(1-(1-\varepsilon)^s)}, \tag{3}$$

where s is the minimal subset size (i.e., for plane estimation $s = 3$). The points of the maximum consensus set are used to estimate by least squares the final coefficients of the discontinuity plane.

If the dataset contains several models (i.e., if points have been measured on several discontinuity planes), RANSAC will find the one with the largest consensus set, i.e., the largest (if the point density is roughly constant). Note, however, that with respect to this plane, the points measured on other planes can be considered outliers (i.e., will likely fall outside the acceptance region). To find all discontinuity planes in the dataset, RANSAC can be reiterated until all points have been linked to a plane or discarded as true outliers (e.g., points measured on vegetation). To this aim, after the final least-squares estimates of the parameters have been computed for a given plane, its inliers are removed from the dataset and the RANSAC search is repeated on the remaining data. In principle, this will lead to the segmentation of the whole dataset, from the

largest to the smallest plane, where the ranking depends on the cardinality of the inlier sets.

The number of iterations grows exponentially with the outlier percentage, as is apparent from Eq. (3). At the beginning, the outlier percentage will be high but will decrease with the iterations: assuming (conservatively) that each plane has approximately the same number of supporting points, it can be evaluated as follows:

$$\varepsilon = 1 - \frac{1}{N_{\mathrm{P}}}, \tag{4}$$

where N_{p} represents the number of planes present in the dataset at that iteration.

Since the probability p must be kept close to 100%, with more than 5–10 planes to extract, the outlier percentage becomes very high and thus the number of iterations makes the solution computationally expensive (see Table 2). Using RANSAC on the whole point cloud is not practical. Hierarchical segmentation of the point cloud at different resolutions can be implemented to tackle this problem (Roncella and Forlani 2005); otherwise, the method can still be used interactively, to speed up the extraction, simply selecting from the point cloud a subset containing a few discontinuities each time. Of course, this takes longer operator time than fully automatic segmentation; on the other hand, it is significantly faster than pinpoint measurements on the DTM (extracting single discontinuities), exploits the expertise of the geologist by restricting the processing to the most significant structures, and can be easily learnt by nonspecialists. In the case studies paragraph, comparisons between discontinuities extraction with both approaches show good agreement. Thus, relatively large areas can be selected since the algorithm can automatically identify the different existing planes, speeding up the whole process: manual identification of each plane, which is often difficult and time demanding, is unnecessary. Moreover, planes selected using the pinpoint approach show a larger dispersion around central orientation values for each family, perhaps due to a less favorable ratio of point accuracy to plane size. On the other hand, selecting too large areas can induce the algorithm to miss minor joint systems and increase computing time.

Selecting subsets of points is easy if their 3D coordinates can be linked to images of the rock surface, i.e., if the point cloud can be back-projected in an image. If the point cloud was generated by photogrammetry, this is straightforward, since all the images used to produce it are obviously consistent (oriented) with respect to the

Table 2 RANSAC iterations required by Eq. (3) assuming ε = percentage of outlier, and accepting a probability p of obtaining at least one (minimal) outlier-free subset

Iteration	Outlier percentage, ε				
	50.0%	90.0%	95.0%	99.0%	99.5%
Probability, p					
99%	34	4,603	36,839	4,605,168	36,841,359
95%	22	2,994	23,964	2,995,731	23,965,857
90%	17	2,301	18,420	2,302,584	18,420,680
80%	12	1,609	12,875	1,609,437	12,875,502

same reference frame. If a laser scanner was used, images acquired on site can be oriented with a space resection by identifying image points on the point cloud features and using their coordinates as GCPs; this is not always easy and does not lead to accurate registration, but it may suffice in most cases. Better results might be achieved using visible targets in both the point cloud and the image, but this is not always feasible. Most laser systems today are equipped with a camera whose orientation and position with respect to the instrumental reference system is calibrated, so that image registration is straightforward.

Once plane extraction is completed, each surface is classified in terms of goodness of fit (mean square error), cardinality, and location of the gravity centre as well as dip and dip direction.

4.3 Interactive Extraction of Planar Surfaces with RockScan

A software package named RockScan has been developed to allow the interactive extraction of planes based on RANSAC. The user loads an oriented image of the rock slope and the point cloud in the background. Through a graphical user interface, regions of interest (ROIs) enclosing one or more discontinuities can be selected by drawing polylines on the image; the corresponding points are selected in the point cloud and inputted to the RANSAC procedure (Fig. 2). For each ROI, the dip and dip direction of all the identified planes are computed. Figure 3 shows an example where several planes were automatically identified from a single region. The user can take advantage of the RANSAC procedure in two different ways: with single plane extraction (SPE) just one discontinuity (the largest in the ROI) will be extracted; with multiple plane extraction (MPE), one or several planes may be extracted, depending on the processing parameter settings. In other words, SPE runs RANSAC once over the dataset in the ROI while MPE runs RANSAC several

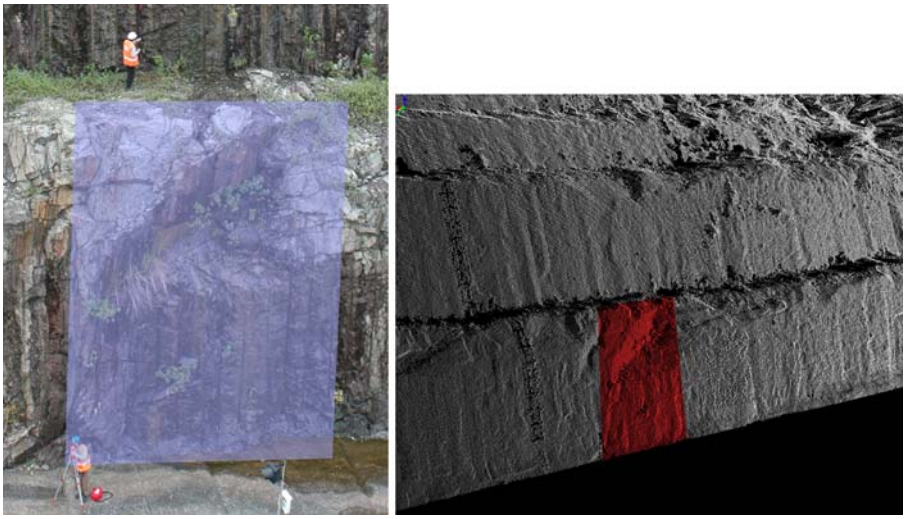

Fig. 2 Cloud point selection and corresponding selection on the DTM

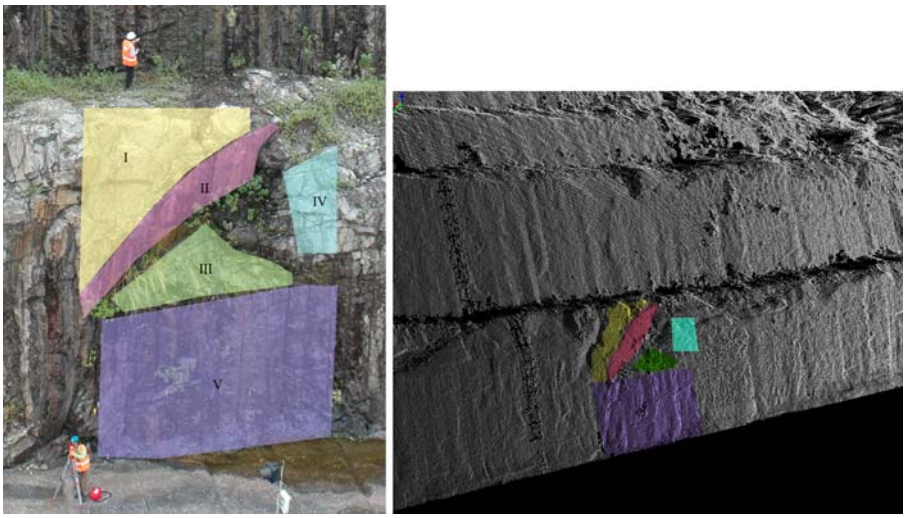

Fig. 3 Rock face automatic segmentation of the previously selected area

times, as pointed out in Sect. 4.2. Therefore, SPE is more time consuming but the user has full control over the outcome; MPE is more productive (the user can contour a bigger area, with several discontinuities) but the results change with the settings of the extraction parameters and must therefore be checked by the operator.

With a few trials the user can adapt the acceptance threshold in RANSAC to account for measurement noise, the resolution of the point cloud, and the roughness of the discontinuity surface: values in the range from 5 to 20 cm were found to be appropriate in the cases shown later. The outlier percentage and number of iterations are computed adaptively, as described in Roncella and Forlani (2005). The discontinuity parameters are outputted in appropriate format for the ensuing geometric modeling of the rock face.

5 Test Cases

The semi-automatic extraction procedure has been applied to various sites. Arnad (Italy) was selected as a pilot site (Voyat et al. 2006). Two additional sites, Longeborne in Switzerland and Mount Granier in France, were chosen to evaluate the flexibility of photogrammetry in different contexts; results on several sites along a motorway in Malaysia, where laser scanning was applied, are also reported.

Once the rock mass has been characterized, it is modeled to determine the stability conditions. Fractured rock masses can be regarded as an assemblage of many individual polyhedral blocks. The modeling is performed in two phases: geometric modeling and mechanical modeling.

The geometric discretization of a rock mass into blocks is based on an ideal perfect discontinuous medium. In this study, geometrical modeling was Resoblok Héliot (1988a, b). Its procedure is to follow the tectonic history of the formation; a

continuous medium is transformed into a block system. Joints can be introduced in a deterministic way, as in the case of faults or singular discontinuities directly detected on site; the joint sets are automatically generated in a statistic way on the basis of surveyed discontinuities, by means of statistical distribution.

Discontinuities can be located in the modeling space at a specified position when the discontinuity is known, visible, and sampled, or by a statistical model in all other cases by considering the distribution frequencies of the discontinuity spacing and persistence.

The deterministic analysis is based on the orientation, position, and persistence of the fractures; a single discontinuity can be considered either completely persistent, and therefore crossing the overall model, or not completely persistent. The joint sets (derived from statistic analysis) are represented on the basis of the principal orientation, mean spacing, and persistence. The code randomly defines the discontinuity position in the rock mass. Discontinuity orientations and spacing are generated in accordance with the statistical distribution determined by analyzing in situ measurements with statistic classical methods. The persistence of the joints is performed by generating a hierarchy of the probabilistic distribution of the fracturing by taking into account the relationships between the joint sets directly observed by the survey.

Persistence is determined by measuring the discontinuity trace length: RockScan, coupling images, and the point cloud data together allow a true 3D estimation of the trace lengths. In other words, a virtual window sampling or a virtual scanline can been carried out when applying ISRM (1978) suggested procedures.

On the basis of this kind of geometrical reconstruction of the rock mass it is then possible to carry out the stability analysis of the rock mass either with LEM by using the code called Block Stability Analysis (BSA in this work, LAEGO-INERIS 1999) or with DEM (3DEC, in this work, Itasca 1998).

5.1 Arnad, Italy

At the pilot site of Arnad (Aosta Valley, North West Italy), the rock face shows subvertical pillar-shaped structures separated from one another by narrow channels connected to structural elements. These structures do not show remarkable signs linked to the presence of water. The slope is 150 m long and 90 m high and its orientation is 238°/80°. The local geology is characterized by light-brown gneiss intercalated by metabasitic lenses parallel to the schistosity (Sc).

A traditional geostructural survey was performed (Table 3) in order to compare and validate the results. Both horizontal scanlines at the base of the slope and vertical scanlines in different slope areas were executed (Fig. 4). About 190 discontinuities were measured, and their analysis led to the identification of five more frequent sets and three sets with larger spacings. The measured data also included persistence, spacing, and roughness.

The point cloud was generated from a photogrammetric survey. A set of 37 ground control points (GCP) and check points were determined on the rock face by a reflectorless total station. Six images were acquired with a Nikon D100

Table 3 Traditional survey results

Family	Orientation (°)		Persistence (m)		Spacing (m)	
	Dip	DD	Min	Max	Min	Max
Principal						
Sev1	75	140	20	100	0.5	10
			40		5	
Sev2	75	195	20	80	0.5	10
J6			30		5	
J1	78	238	30	80	4	8
			50		6	
J2	10	50	4	15	0.5	10
			10		5	
J7	35	295	5	30	0.5	10
			20	50	2	
Secondary						
J3	40	250	4	–	0.5	–
			6		1	
J4	35	25	4	10	–	–
			7			
J5	55	160	6	15	2	–
			8		4	

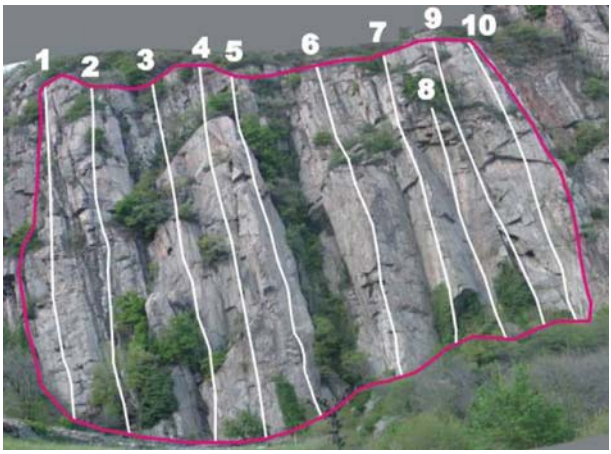

Fig. 4 Traditional scan lines on the Arnad slope

(6 Mpixels, pixel size = 7.8 μm) with an 18 mm lens from a distance ranging from 50 to 70 m (ground resolution from 2.1 to 3 cm). Residuals on the GCPs from the block adjustment were around 4 cm. The point cloud was generated from a single stereo pair by digital image correlation using the software Virtuozo™; about 1.3

Fig. 5 Plane identification with RockScan

millions points were obtained on a grid with a cell spacing of 5 cm; overall, the area surveyed is about 60 m high and 75 m wide.

Using RockScan to extract the discontinuities, the influence of the size of the ROIs contoured in the image on the number of the extracted planes and the values of their parameters was also investigated (Fig. 5 shows an example SPE). At first, using an SPE approach (Fig. 6a) 177 planes were extracted and identified by RANSAC. Next bigger ROIs, contouring several discontinuities (Fig. 6b), were again processed by RANSAC: 111 planes were identified by the MPE procedure.

Both sets of planes were projected onto a stereographic net and a statistic analysis performed. The comparison between the two stereo nets (Fig. 7) shows that results by RANSAC using SPE and MPE are in good agreement.

Finally, a comparison between the traditional compass survey and photogrammetric results was carried out and is summarized in Table 4. As is apparent, most of the discontinuity families were identified with a good correspondence. Family J2 was not identified since it is a subhorizontal family that can hardly be captured by the photogrammetric survey because of the unfavorable incidence angle of the imaging geometry to the surface: the planes of the family are either occluded or compressed into a few pixels in the images, taken at the base of the slope.

One more family (J8 subvertical) was identified by the photogrammetric restitution whereas it was neglected by the traditional survey. In the traditional survey this set was confused with joint set J1, which had a similar orientation: the geologist did not sample the discontinuity belonging to J8 due to difficulties in accessing the rock slope. However, joint set J8 plays an important role in the slope stability condition since it determines the formation, together with J6, of the columnar structure that is characteristic of the right side of the slope.

A geometrical model of the site based on the above described survey was set up by applying the code Resoblok. The obtained model is composed by 1,952 blocks, reproducing a rock mass volume of 50 × 70 × 50 m.

Stability analyses were performed, assuming shear resistance determined by laboratory tests. Direct shear test have been performed on joints showing a peak

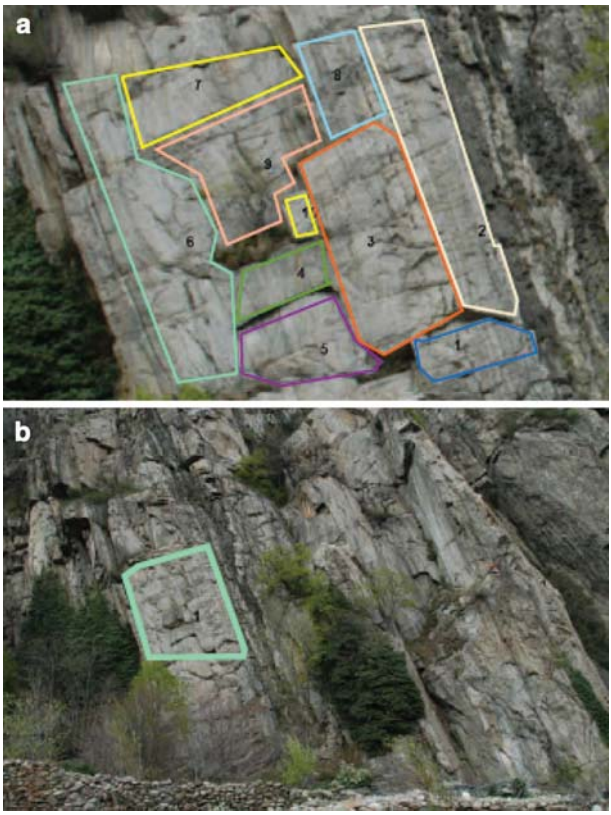

Fig. 6 Single plane extraction (SPE) and multiple plane extraction (MPE) selection

friction angle equal to 55° and a residual friction angle of 40°. Rock joint persistence varied between 30% and 70%. All joint sets reported in Table 4 were considered in the analysis.

The results from the different stability analyses were compared with in situ observations and showed that the kinematic mechanism is of toppling and sliding nature along the subvertical discontinuities, as pointed out by the on-site measurements. In fact, planar sliding and 3D toppling and sliding along J1 SCv1 and along J6–J8 and J7–J8 were computed by BSA. Blocks identified by the intersection between J7 and J8 slide along an inclination of 35° (Fig. 8) and consequently are in stable conditions due to friction. Blocks determined by the intersection between J6 and J8 are toppling or sliding along a much steeper intersection. These kind of blocks are unstable when residual friction angle is considered and cohesion is equal zero, and they can slide or topple depending on the base plane orientation. The base is, in fact, determined by J2, which is nearly horizontal and tilting between a dip direction of 50° and 230°. When J2 is close to the rock slope direction (240°) a sliding phenomenon can occur, whereas when it is around 50° toppling is the most possible kinematics. The computed kinematics

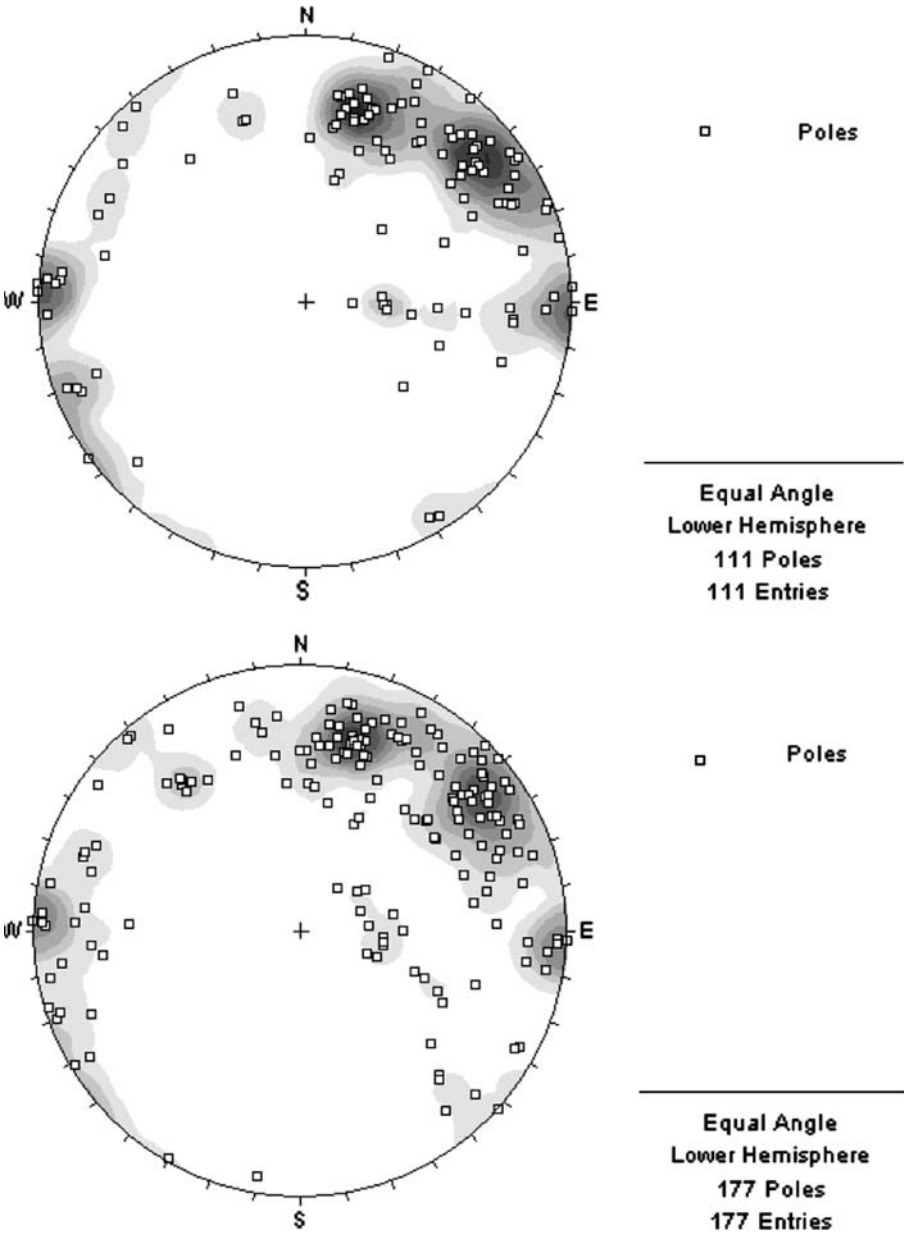

Fig. 7 Comparison of results using the single plane extraction (SPE) and multiple plane extraction (MPE) options

correspond geometrically to blocks observed at the base of the slope and with the instability traces on the slope. The global volume of computed unstable blocks was 4,000 m^3 as the volume of the blocks measured at the base of the slope.

Table 4 Discontinuity joint set orientation obtained with the traditional and photogrammetrical methods

Families	Traditional survey		RockScan	
	Dip	DD	Dip	DD
Scv1	75	140	78	143
J6–Scv2	75	195	73	200
J1	78	238	81	238
J2	10	50	*	*
J7	36	295	39	283
J8	*	*	89	271

*Joint set not identical

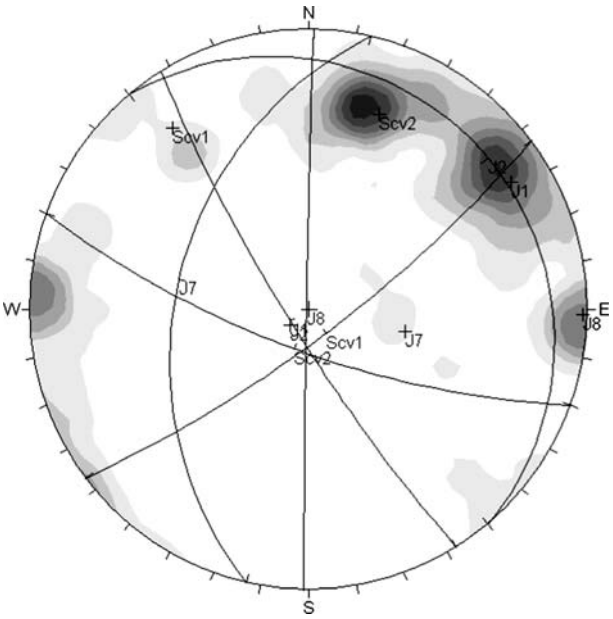

Fig. 8 Stereographic projection of data obtained by photogrammetric survey utilized for the kinematic analysis

Figure 9 shows the Resoblok model of the slope and the BSA simulation. The figures show some example of unstable blocks determined by the intersection of the joint sets described above.

5.2 Mount Granier, France

Mount Granier forms the northern part of the Chartreuse Massif and is located at the boundary of the French departments of Isère and Savoy, in the Chambéry municipality (Fig. 10). Mount Grainer is made of calcareous rock lying on a marble-calcareous level dipping 15° toward the south east.

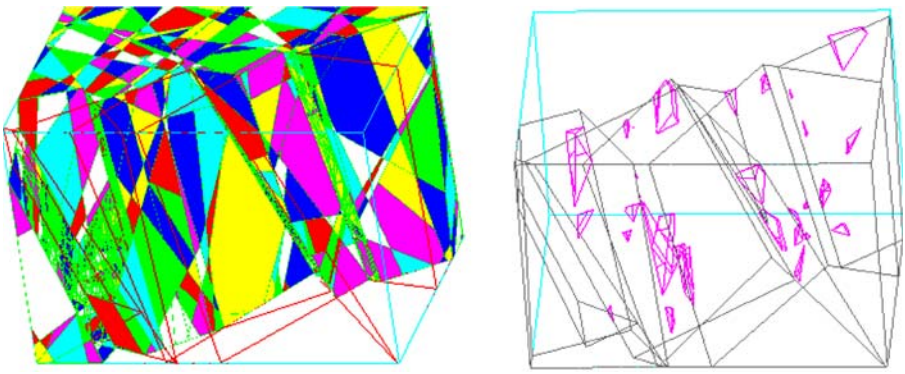

Fig. 9 Resoblok model of the rock slope on the left and relative BSA simulation

Fig. 10 Mount Granier slope

In this site no in situ survey could be performed; the photogrammetric survey was executed using nine slightly convergent images provided by the Université Joseph Fourrier of Grenoble. The photographs, taken from a helicopter with a film metric camera UMK 10 with a 100 mm lens, cover the mount's northern side (about 500 m high and 700 m wide); each image, 160 mm × 115 mm wide, was digitized with a resolution of 20 μm/pixel.

Three point clouds were generated on the north face and one on the east face; overall, the point clouds consist of 3.5 Mpts, with average spacing of about 7–10 cm. Orientation of the stereo models in the mapping system was performed using four GCPs provided with a topographic survey by the Université Joseph Fourrier; topographic survey and identification of the points in the images proved difficult, with residuals of about 20 cm.

As in the Arnad case, the influence of the size of the ROI on the discontinuity identification by RockScan was also investigated (Fig. 11). Two hundred and

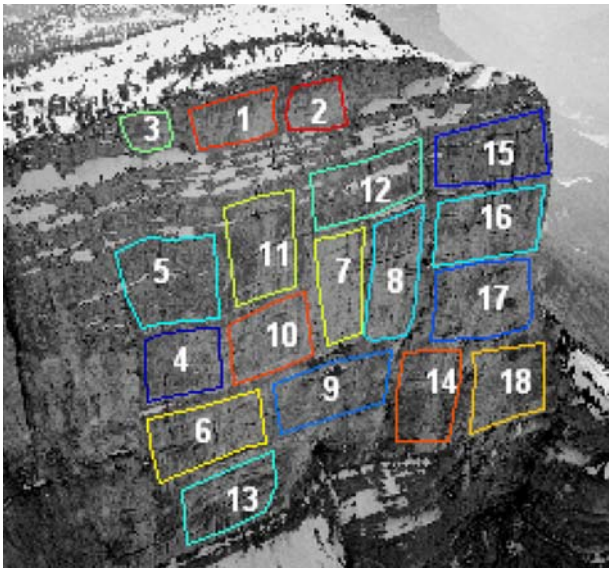

Fig. 11 Multiple plane extraction (MPE) selection

eighty-eight planes were identified by SPE, while 182 planes were determined by MPE. The statistical analysis of the orientation data is shown in Fig. 12; four families were identified in both cases.

Figure 13 shows the sequences performed to set up the Resoblok model of the slope. The model is composed of 3,967 blocks reproducing a rock mass volume of 350 × 700 × 450 m.

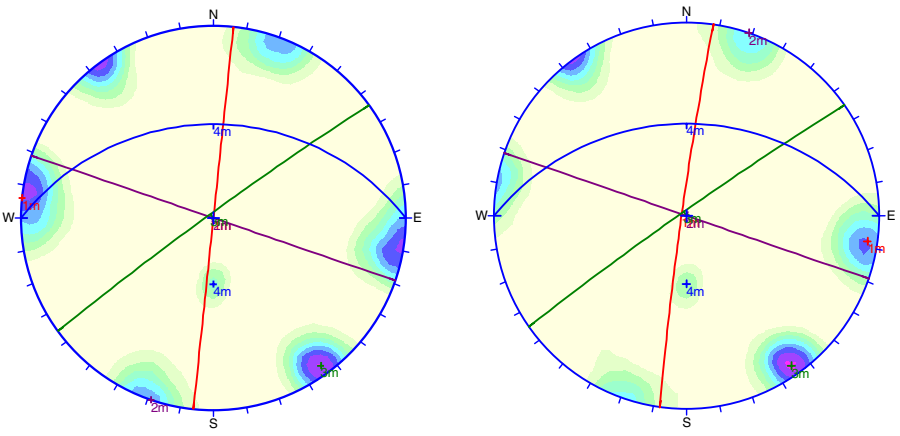

"SPE" "MPE"

Fig. 12 Comparison of results from single plane extraction (SPE) and multiple plane extraction (MPE)

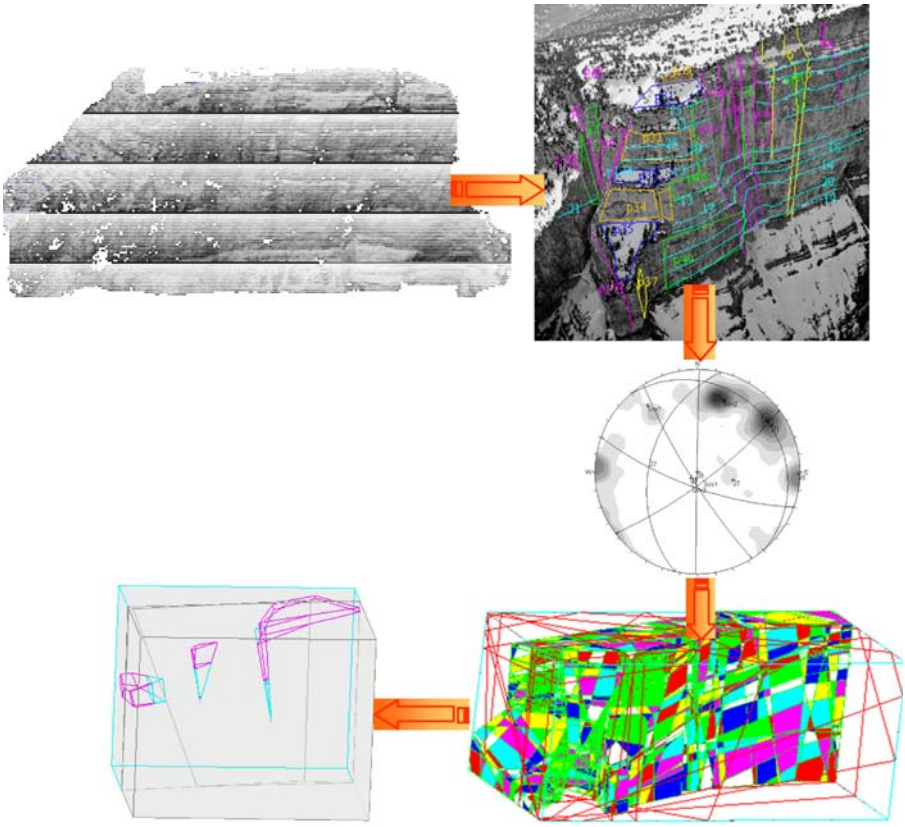

Fig. 13 Mount Granier, complete procedure

BSA stability analysis of the slope was performed, showing that the slope is stable for a friction angle above 43° and cohesion above 30 kPa.

Two kinds of kinematic, planar sliding on subhorizontal planes along joint family 6 and a 3D sliding along sets 3, 5, and 6 (tension cracks), were identified and confirmed by in situ observation.

5.3 Longeborgne, Switzerland

This rock mass is located in the municipality of Bramois, in the Vallis canton, overhanging an ancient monastery called the Ermitage de Longeborgne. The rock slope is located between the Cernesis and the Pennine Alps and it has been characterized by several instability phenomena (Fig. 14).

The Longeborgne rock slope mainly consists of quartzite that composes massive conglomerates alternating with stratified sands. Since the sands are more weathered materials than the conglomerate, they induce the formation of large cavities.

The presence of joint sets with direction west south west–east north east with a dip direction of about 160° determines the formation of rock wedges, clearly

Fig. 14 Longeborgne (CH) rock slope

observable on the slope. A regularly spaced and subhorizontal main schistosity is also apparent. Schistosity is often coincident with stratification planes. The other joint planes are subvertical, forming large columnar rock blocks.

The site has two faces: the larger is south oriented and visible only from the bottom of a narrow valley, about 100 m below: the perspective is, therefore, unfavorable, with the wall compressed into a few pixels; the second is west oriented and can be imaged from the same height but only from the north side, with a rather poor imaging geometry. A topographic survey of the site provided 27 well-identified GCPs for image orientation and, on the west side, 200 points automatically taken in a grid-like fashion by a reflectorless total station, for independent checking of the photogrammetric survey. Images were taken with a Nikon D100 a with a 105 mm lens for the south slope and with a 18 mm lens for the West slope. Shooting distance was about 120 and 20 m, respectively. Due to the aforementioned limitations, Virtuozo proved unsuitable for DTM generation with images of the south face; software based on the least-squares matching was therefore implemented and applied to both faces. In the following, only the results for the west face are described, where check points were available. The surveyed face is about 30 m wide and 25 m high; three series of images were taken from distances between 48 and 57 m (object resolution about 2.3 cm). Block orientation with Photomodeler gave discrepancies on 18 check points of 1.5 cm in all coordinates. Point cloud and DTM generation were performed with a multi-image version of the least-squares matching algorithm. More than 100,000 pts with a point spacing of about 8 cm were obtained from six images. The root-mean-square (RMS) of the deviations for the 200 check points projected over the DTM was 3 cm, with a maximum difference of 4 cm.

SPE and MPE yielded 126 and 54 planes, respectively. Once again, we obtained similar results with the two procedures. Four main sets were identified: three subvertical families with a dip above 80° and one subhorizontal family. These results were confirmed by the larger-scale observation, although a specific traditional survey could not be performed.

5.4 Granitic Rock Slope, Malaysia

Laser scanning was applied to the survey of eight rock slopes along a highway in Malaysia (Ferrero et al. 2007).

The rock slopes all expose a porphyritic, biotite granite with quartz and feldspar phenocrysts set in a medium- to coarse-grained matrix (0.5–1.5 cm in size) of quartz, biotite, alkali, and plagioclase feldspars. Quartz veins, aplite dykes, and pegmatites of variable orientations and sizes are also present within the granite bedrock in places. A variety of structural discontinuity planes are present within the granitic bedrock and include exfoliation planes, shear and tensional joints, and faults. The faults are of various lengths and marked by singular shear planes or narrow to broad (<5 m wide) shear zones as well as brecciate bedrock. The discontinuity planes are of variable orientations as well as spacing and extent. Fresh to slightly weathered granitic bedrock (rock mass weathering grades I and II) is only exposed in the lower benches of the slope cuts; the upper benches are excavated in moderately to completely weathered bedrock (rock mass weathering grades III to VI).

The size of the slopes varies from about 40 × 40 m to 750 × 135 m. Each was surveyed by laser scanning with a Riegl LMS-Z420i coupled to a calibrated Nikon D70 digital camera.

In each slope two different survey resolutions were used:

- general description of the slope: a point spacing of 5 cm and images taken with a 20 mm calibrated lens;
- detailed survey in areas, about 10 m × 10 m in size, representative of the whole rock structure, with a point spacing of 1 cm and images taken with a 84 mm calibrated lens.

Point cloud orientation in the mapping system was performed by surveying with GPS and a total station with either the reflecting targets used to connect different scans or as the topographic ones to connect theodolite stations.

A geological-geostructural mapping was carried out for the eight slopes in order to describe the rock mass and define geostructural domains.

Due to rock surface characteristics, plane extraction with RockScan (Fig. 15) was restricted to areas where both image resolution and point cloud density enabled the identification of meaningful discontinuities. In the following, results are reported for one slope only (Figs. 16 and 17).

Figure 18 shows a comparison between the orientation data obtained by the geological traditional survey done by compass and the subsequent statistical analysis on the pole density contour data for the determination of the major joint sets. Two main families, both subvertical dipping, north (J2) and north West (J1),

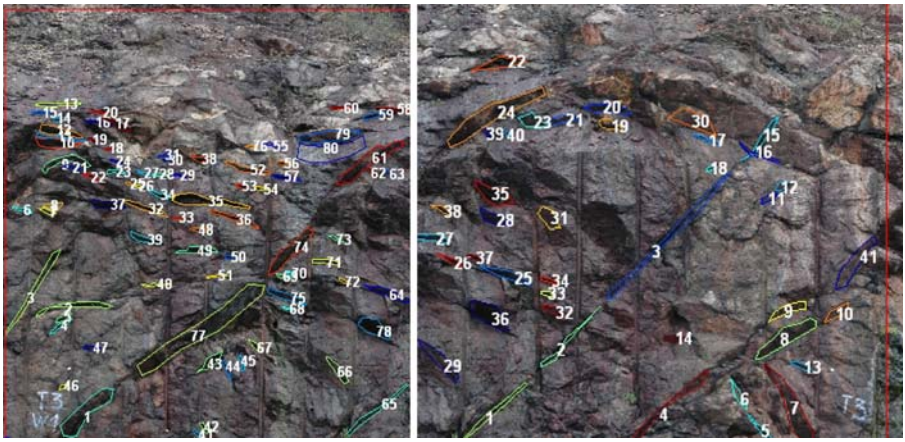

Fig. 15 Planes extraction with RockScan

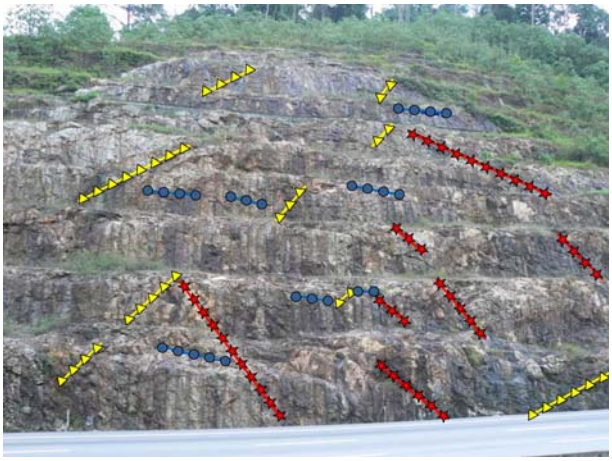

Fig. 16 Joint set localization (*J1-triangles*, *J3-circles*, *J4-stars*) on slope W01

respectively, were identified, with both approaches, validating the laser scanner survey and the subsequent data analysis.

By using the laser scanner DTM a larger number of poles (121) were measured in comparison with the traditional survey (46) since a larger area (10 × 10 m^2) could be observed whereas the traditional survey could only cover the accessible rock slope along the scan line (about 3 m high). The higher number of data is possibly the cause of the less disperse pole distribution resulting from the laser scanner data in comparison with the compass data. Moreover two more sets are observed oriented 72°/75° (J3) and 53°/146° (J4) and, consequently, stability analyses were performed considering the presence of all four sets.

All joint set have been considered in their residual condition in order to take weathering action into account by taking a shear strength angle of 32°.

For the vertical berm, various kinds of removable blocks have been identified:

1. Planar sliding on joint set 4 (146/53) of several small blocks (maximum computed volume of a single block less than 1 m^3, global volume of 2.5 m^3).
2. Tridimensional sliding along the intersection 175°/89° and 146°/53° towards E with tension crack (309°/80°).

The observation of local instabilities allows the recognition of a wedge sliding at the intersection between joint sets and a planar sliding on joint 146°/53°, confirming the computational results.

A geometrical model of the site based on the above described survey was set up by applying the code Resoblok (Fig. 18). The obtained model was composed of 1,265 blocks, reproducing a rock mass volume equal to 100 × 40 × 40 m.

Figure 18 shows the Resoblok model set up on this basis and the sliding phenomena computed by the BSA that have determined the same kind of kinematics as observed in situ.

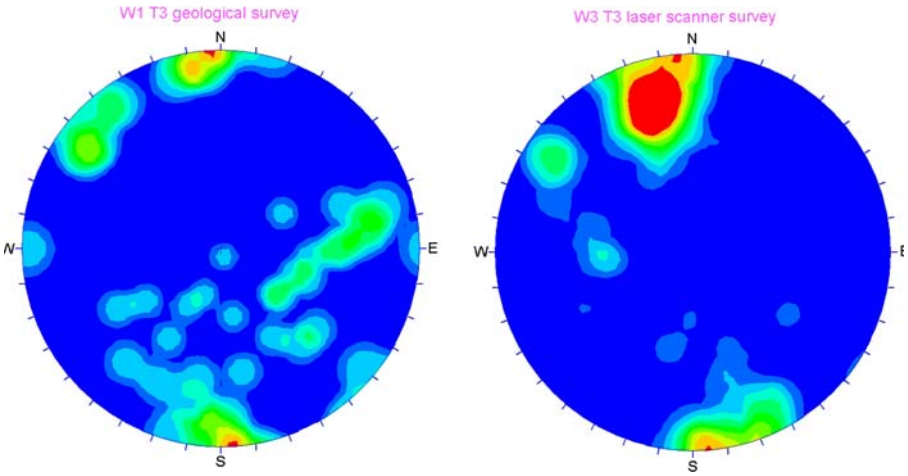

Fig. 17 Pole density contour determined by geostructural traditional survey (**a**) and by laser scanner and RockScan survey (**b**) on the scanline T3

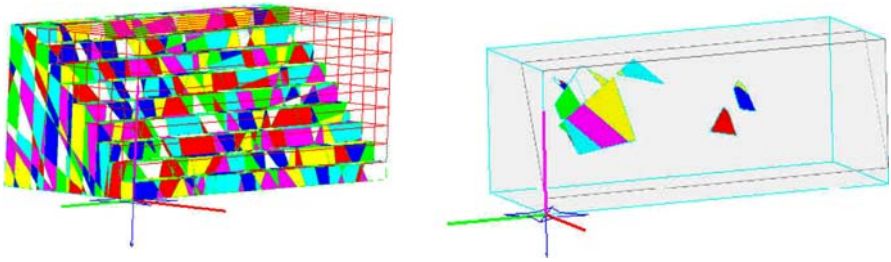

Fig. 18 Resoblok model of slope W01 and the BSA unstable block computation

6 Conclusions

A method for rock discontinuity mapping that relies on accurate high-resolution survey technologies and on segmentation algorithms has being developed in this work. Interpolation techniques to model daylight discontinuities and to compute their dip and dip direction have also been studied. The main advantages of this approach are the large number of data that can be safely and rapidly collected even in difficult environments and the possibility to utilize semi-automatic tools for discontinuity identification and measurement.

As far as data acquisition is concerned, photogrammetry and laser scanning are the best technologies available today.

The survey must be carefully designed to ensure reliable quality standards that are able to capture all relevant discontinuity features. As far as methodology is concerned, the results of a series of simulations is also shown, highlighting the influence of point measurement accuracy and sampling density on the accuracy of dip and dip direction determination, accounting for the shape and orientation of the discontinuity plane. The paper proposes a methodology to quantify the minimum number of points to be acquired to reach a given precision in the determination of the plane orientation. This method can be usefully applied in the survey design phase in order to optimize the survey in terms of the number of required photographs, shooting distances, camera optics, etc.

The paper proposes a semi-automatic procedures, implemented in the code RockScan, which represents a convenient operational tool. Discontinuities are extracted by detecting plane surfaces directly from the point cloud by using a RANSAC-based segmentation algorithm. The user task is restricted to contouring roughly on the image an area containing one or more discontinuities, detected by the iterative application of RANSAC for the selected points. Several tests on different sites show that the size of the area to be contoured is not critical to the output, although for computational reasons the procedure cannot yet handle a whole rock face. The paper also shows as the plane equation identification based on simple interpolation algorithm can lead to major estimation mistakes since it is unable to handle with outliers. This fact confirming the opportunity to use segmentation algorithm.

Due to efforts underway in laser data processing (feature recognition and extraction, automatic modeling, etc.) further progress can be expected in terms of the automation level of the segmentation for methods working directly on the point cloud; methods working on surface normals to the DTM patches may improve due to better surface meshing and clustering techniques. Both approaches need a statistical analysis of the orientations in a polar plot in order to identify discontinuity families, and consequently need consistent sample data.

Three sites surveyed photogrammetrically and one with laser scanning were presented; in two cases (Longeborgne and Mount Granier) no on-site traditional survey would have been possible without taking severe risks. At all sites, which differ in terms of size from tens to hundreds of meters, their rock surface characteristics, and the technology used to produce the point cloud, results were in good agreement with the available information.

The proposed method guarantees a large number of data that can be utilized to reconstruct the rock mass geometrically. Some examples of rock mass geometrical reconstruction by applying the code Resoblok are also provided in the paper, showing that a good geometric reconstruction can yield good results in the evaluation of rock mass stability conditions when discontinuous methods are adopted for the rock mass modeling.

Acknowledgments This work has been supported by Valle d'Aosta Region within the research program Interreg III A "Rock Slide Detect" and by the Interreg III B Alpine Space project "ClimChAlp". The data on Mount Granier were kindly provided by the Université Joseph Fourrier, Grenoble.

References

Barla G, Barla M (2000) Continuum and discontinuum modelling in tunnel engineering Građevinar 52, Num 10

Barla G, Barla M (2001) Continuo e discontinuo nella modellazione numerica dello scavo di gallerie. Gallerie e grandi opere sotterranee n.61

Besl PJ, McKay ND (1992) A method for registration of 3-D shapes. IEEE Trans Pattern Anal Mach Intell 14(2), February

Birch JS (2006) Using 3DM analyst mine mapping suite for rock face characterization. In: Tonon F, Kottenstette J (eds) Laser and photogrammetric methods for rock face characterization. ARMA Golden, Colorado

Crosta G (1997) Evaluating rock mass geometry from photographic images. Rock Mech Rock Eng 30(1):35–58

Cruden DM (1977) Describing the size of discontinuities. Int J Rock Mech Min Sci Geomech Abstr 14:133–137

Davis JC (1986) Statistics and data analysis in geology. Wiley, New York, p 646

Dolan JP (2006) Rapidly acquiring and analyzing rock mechanic data using laser scanning technology workshop on laser and photogrammetric methods for rock face characterization. ARMA, Golden, Colorado

Felus YA (2006) On linear transformations of spatial data using the structured total least norm principle. Cartogr Geogr Inf Sci 33:195–205

Feng Q, Sjogren P, Stephansson O, Jing L (2001) Measuring fracture orientation at exposed rock faces by using a non-reflector total station. Eng Geol 59:133–146

Ferrero AM, Migliazza MR, Giani GP (2004) Analysis of the stability condition of tunnels: comparison between continuous and discontinuous approaches. Int J Rock Mech Geomech Abstr 41(3):483

Ferrero AM, Forlani G, Migliazza MR, Roncella R, Grasso P, Rabbi E (2007) Analysis of stability conditions of rock slopes based on laser scanner surveys. XI ISRM Congress Lisbon

Fischler M, Bolles R (1981) Random sample consensus: a paradigm for model fitting with application to image analysis and automated cartography. Commun Assoc Comp Mach 24(6):381–395

Gaich A, Schubert W, Pötsch M (2004) Reproducible rock mass description in 3D using the JointMetriX3D system. In: Schubert W (ed) Proceedings of EUROCK 2004 and 53rd geomechanics colloquium. Salzburg, Austria, pp 61–64

Gaich A, Pötsch M, Schubert W (2006) Basics, principles and applications of 3D imaging systems with conventional and high-resolution cameras. In: Tonon F, Kottenstette J (eds) Laser and photogrammetric methods for rock face characterization. ARMA Golden, Colorado

Golub GH, Van Loan CF (1989) Matrix computations, 2nd edn. The John Hopkins University Press, Baltimore

Grenon M, Lemy F, Hadjigeorgiou J (2004) Fracture modelling based on input data from line mapping and image analysis. In: Schubert W (ed) Proceedings of EUROCK 2004 and 53rd geomechanics colloquium. Salzburg, Austria, pp 445–448

Grün A (1985) Adaptive least squares correlation: a powerful image matching technique. S Afr J Photogramm Remote Sens Cartogr 14(3):175–187

Grün A, Baltsavias EP (1988) Geometrically constrained multiphoto matching. Photogramm Eng Remote Sens 54(5):663–671
Hadjigeorgiou J, Lemy F (2005) Développement d'un système d'analyse d'images pour la caractérisation des massifs rocheux. Rapport soumis à l'Institut de recherche Robert-Sauvé en santé et sécurité du travail (IRSST). (Rapport R-414), pp 46
Hadjigeorgiou J, Lemy F, Côté P, Maldague X (2003) An evaluation of image analysis algorithms for constructing discontinuity trace maps. Rock Mech Rock Eng 36(2):163–179
Hagan TO (1980) A case of terrestrial photogrammetry in deep-mine rock structure studies. Int J Rock Mech Min Sci 15:191–198
Harrison JP (1993) Improved analysis of rock mass geometry using mathematical and photogrammetric methods. Ph.D. thesis, Imperial College, London, UK
Héliot D (1988a) Conception et Réalisation d'un Outil Intégré de Modélisation des massifs Rocheux Fracturés en Blocs. Ph.D. Thèse, Institut National Polytechnique de Lorraine
Héliot D (1988b) Generating a blocky rock mass. Int J Rock Mech Sci Geomech Abstr 25(3):127–138
ISRM Commission for Standardization of Laboratory and Field Tests (1978) Suggested methods for the quantitative descriptions of discontinuities in rock masses. Int J Rock Mech Min Sci 15(6):319–368
Itasca Consulting Group (1998) Minnepolis, MN, 3DEC, ver. 2
Jing L (2003) A review of techniques, advances and outstanding issue in numerical modelling for rock mechanics and rock engineering. Int J Rock Mech Min Sci, 40 (journal review article)
Jing L, Hudson JA (2002) Numerical methods in rock mechanics. Int J Rock Mech Min Sci 39:409–427 (civil zone review paper)
Kemeny J, Post R (2003) Estimating three-dimensional rock discontinuity orientation from digital images of fracture traces. Comput Geosci 29(2003):65–77
Kemeny J, Monte Handy J, Thiam S (2003) The use of digital imaging and laser scanning technologies in rock engineering. In: International symposium on the fusion technology of geosystem engineering, Rock engineering and geophysical exploration, Seoul, Korea, 18–19 November
Kemeny J, Turner K, Norton B (2006) LIDAR for rock mass characterization: hardware, software, accuracy and best-practices. In: Tonon F, Kottenstette J (eds) Laser and photogrammetric methods for rock face characterization. ARMA Golden, Colorado
Kraus K (1993) Photogrammetry, vol 1, 4th edn. In: Dummler F (ed), Bonn. ISBN:3-427-78684-6
Kulatilake PHS, Wathugala DN, Stephansson O (1993) Joint network modelling with a validation exercise in Stripa Mine, Sweden. Int J Rock Mech Min Sci 30:503–526
LAEGO-INERIS (1999) Resoblok bg bd bh v4.01 BSA Rapport interne, Ecole des Mines de Nancy
Lemy F, Hadjigeorgiou J (2003) Discontinuity trace map construction using photographs of rock exposures. Int J Rock Mech Min Sci 40:903–917
Lichti DD, Jamtsho M (2006) Angular resolution of terrestrial laser scanners. Photogramm Rec 21(114):141–160
Priest SD (1993) Discontinuity analysis for rock engineering. Chapman & Hall (eds), London, p 472
Priest SD, Hudson J (1976) Discontinuity spacings in rock. Int J Rock Mech Min Sci Geomech Abstr 13:135–148
Priest SD, Hudson J (1981) Estimation of discontinuity spacing and trace length using scanline survey. Int J Rock Mech Min Sci Geomech Abstr 18:183–197
Reid TR, Harrison JP (2000) A semi-automated methodology for discontinuity trace detection in digital images of rock mass exposures. Int J Rock Mech Min Sci 37:1073–1089
Roncella R, Forlani G (2005) Extraction of planar patches from point clouds to retrieve dip and dip direction of rock discontinuities. Proceedings of laser scanning 2005, Enschede, The Netherlands. Int Arch Photogramm Remote Sens 36(3W19):162–167
Roncella R, Forlani G, Remondino F (2005) Photogrammetry for geological applications: automatic retrieval of discontinuity orientation in rock slopes. In: Videometrics IX, electronic imaging, IS&T/SPIE 17th annual symposium, pp 17–27
Slob S, Hack HRGK, van Knapen B, Turner K, Kemeny J (2005) A method for automated discontinuity analysis of rock slopes with 3D laser scanning. Transp Res Rec 1913(1):187–208
Terzaghi RD (1965) Sources of error in joint surveys. Géotechnique 15:287–304
Torr PHS, Murray DW (1997) The development and comparison of robust methods for estimating the fundamental matrix. In: Int J Comput Vis, Kluwer Academic Publishers, Boston, pp 1–33
Tsoutrelis CE, Exadactylos GE, Kapenis AP (1990) Study of the rock mass discontinuity system using photoanalysis. In: Rossmanith HP (ed) Mechanics of jointed and faulted rock. Balkema, Rotterdam, pp 103–112

Vallet J, Skaloud J, Koelbl O, Merminod B (2000) Development of a helicopter-based integrated system for avalanche and hazard management. Int Arch Photogramm Remote Sens 33/B2:565–572 (Amsterdam)

Voyat IH, Roncella R, Forlani G, Ferrero AM (2006) Advanced techniques for geo structural surveys in modelling fractured rock masses: application to two Alpine sites. In: Tonon F, Kottenstette J (eds) Laser and photogrammetric methods for rock face characterization. ARMA Golden, Colorado

Zhang L, Einstein HH (1998) Estimating the mean trace length of rock discontinuities. Rock Mech Rock Eng 31(4):217–235

Zhang L, Einstein HH (2000) Estimating the intensity of rock discontinuities. Int J Rock Mech Min Sci 37:819–837